ECCOMAS Congress 2016
VII European Congress on Computational Methods in Applied Sciences and Engineering
M. Papadrakakis, V. Papadopoulos, G. Stefanou, V. Plevris (eds.)
Crete Island, Greece, 5–10 June 2016

NUMERICAL SIMULATION OF NONLINEAR FREE SURFACE WATER WAVES USING A COUPLED POTENTIAL FLOW-URANS/VOF APPROACH

Bülent Düz[1*], Tim Bunnik[1], and Geert Kapsenberg[1]

[1]Maritime Research Institute (MARIN)
P.O. Box 28, 6700AA, Wageningen
The Netherlands
e-mail: {b.duz,t.bunnik,g.k.kapsenberg}@marin.nl

Keywords: Nonlinear free surface water waves, One-way coupling of potential and viscous flow models, Focusing wave events, Waves on sloping bottom, Survey on wave models.

Abstract. *This paper first presents a comparison particularly in terms of accuracy between four nonlinear potential flow models for simulation of nonlinear free surface water waves. The performance of the wave models is compared in five test cases in 2D for which measurement data was also available. Three cases involved wave groups propagating over a flat bottom and producing a focusing event, and two cases involved irregular waves propagating over sloping bottom. After the comparison study, one of the potential flow solvers was selected for one-way coupling with a viscous flow solver. Details of this coupling are presented along with some information about the viscous flow solver in question. Here strong suits of both solvers are utilized to simulate nonlinear water waves in an accurate and efficient manner. Even though only simulating nonlinear waves is discussed in the paper, this work was considered as a stepping stone to later focus on hydrodynamic wave loading on structures and wave-structure interaction using this coupling. In the end results showed that such a coupling can indeed be a valuable tool to study wave motion. In all the simulations, comparison with the measurements demonstrated good agreement, and the convergence behavior of the coupled solver was acceptable.*

*Address all correspondence to this author.

1 INTRODUCTION

Numerical simulation of nonlinear wave-wave, wave-bottom and wave-structure interaction is a challenging endeavor. Even though a myriad of numerical models have been available to investigate these problems, current levels of computational power require making smart decisions to have a balance between accuracy and efficiency. In typical wave-structure interaction applications, viscous effects are generally important near the structure and in regions of strong wave breaking. Naturally a domain decomposition strategy comes to one's mind, where viscous flow solvers are used only in areas where viscous effects may be important, and potential flow models (or other economical but sufficiently accurate models) are used in the rest of the domain. For fully nonlinear, multi-phase and unsteady CFD computations ReFRESCO [1] has been extensively used at the Maritime Research Institute in the Netherlands (MARIN) (for information visit http://www.refresco.org). In order to find a wave model that can be used in combination with ReFRESCO, we first conducted an inventory study on some of the existing codes. The functionalities and performances of the codes were analyzed in various test cases. Then one of these codes was chosen for one-way coupling with ReFRESCO, and the results of this coupling are presented.

Domain decomposition is not the only application area for the potential flow models. These models can also be used to study statistics of extreme waves, reproduce basin waves in a numerical environment, and calculate kinematics underneath waves which then can be used to calculate forces using Morison type equations.

After a detailed survey on the existing codes, four were selected for consideration. Below some information about these codes is given, and some of their features are listed in Tab. 1.

1. HAWASSI (LabMath Indonesia - University of Twente)
   The acronym HAWASSI stands for Hamiltonian Wave-Ship-Structure Interaction, and the code was developed at LabMath Indonesia and the University of Twente. Programming language is MATLAB. The website http://hawassi.labmath-indonesia.org contains information about the software and its functionalities. HAWASSI is not open source, but a demo version with limited functionalities can be downloaded from the website. The software comes in two versions: HAWASSI-AB (Analytic Boussinesq) and HAWASSI-VBM (Variational Boussinesq Model). In this work only HAWASSI-AB was used, and it is simply referred to as HAWASSI in the remainder of this document. For more information about the model, see [2, 3, 4, 5].

2. SWASH (Delft University of Technology)
   The acronym SWASH stands Simulating WAves till SHore. This open source code has been developed based on the work of [6, 7, 8, 9]. The source code was written in FORTRAN 90 and can be downloaded from http://swash.sourceforge.net, which also contains a detailed description of the software and its functionalities. SWASH can be used freely under the terms of the GNU General Public License, and it can be implemented on Microsoft Windows, Linux, Unix and Mac OS/X, provided a Fortran 90 compiler is available.

3. OceanWave3D (Technical University of Denmark)
   OceanWave3D is a fully nonlinear and dispersive potential flow model. It is distributed under the GNU General Public License. The base code was developed at DTU Mechanics between 2006 and 2008 by Allan P. Engsig-Karup, and was entirely rewritten at DTU

Informatics between 2008 and 2011 (current version) by Allan P. Engsig-Karup with contributions from various researchers. The model is described in [10]. Even though the software exists in several versions (FORTRAN 90 and C++), only the FORTRAN 90 version has been made available to public. The source code can be downloaded from https://github.com/apengsigkarup/OceanWave3D-Fortran90.

4. HOS-NWT (École Centrale de Nantes)
   HOS-NWT is a Numerical Wave Tank based on the High-Order Spectral (HOS) method. It has been developed at École Centrale de Nantes, and is currently used in several research projects. The source code is written in FORTRAN 90 and can be downloaded from https://github.com/LHEEA/HOS-NWT. The software is distributed under the terms of the GNU General Public License. The description of the model can be found in [11, 12].

2 RESULTS FROM THE COMPARISON OF THE WAVE MODELS

In this section we present the results from the simulations with HAWASSI, SWASH, OceanWave3D, and HOS-NWT. We consider five test cases for which measurement results are also available from MARIN. The tests consist of three wave groups propagating over a flat bottom, and two irregular waves propagating over a slope. The details of the tests will be given in the corresponding section.

In the experiments a piston-type wavemaker is used at one end of the basin to generate waves. The motion, velocity and acceleration of the wavemaker was available from the experiment. At the other end of the basin a beach is installed to minimise reflections. The wave elevation was measured at various stations in the basin. All the data was provided at 50Hz.

The numerical simulations were all carried out in 2D. The waves are generated using the information from the piston-type wavemaker in SWASH (velocity of the wavemaker), OceanWave3D (velocity of the wavemaker) and HOS-NWT (motion of the wavemaker). With HAWASSI

	Kinematics	Bathymetry	Workaround for wave breaking	Parallelization	Wave generation		
					Piston	Flap	Time trace
SWASH				(MPI)			
OceanWave3D				Not yet public! (MPI)			
HOS-NWT	Available after post-proc.		Work is ongoing!				
HAWASSI	Available after post-proc.						

Table 1: Features of the codes selected for comparison. The version numbers of the codes are: SWASH2.00, HOS-NWT1.1, OceanWave3D0.99, and HAWASSI1.0. SWASH, HOS-NWT and OceanWave3D are open source, and capable of running 3D simulations. Using HAWASSI requires a licence, and only 2D simulations can be performed with this software. Green indicates that the code has the corresponding feature while red indicates that it does not or the work is ongoing. Kinematics: The code calculates the kinematics at each time level during the simulation in the entire domain. Bathymetry: Effects of bathymetry are included in the model. Workaround for wave breaking: In case of wave breaking, the code does not stop the simulation, but rather activates an *ad hoc* numerical workaround for continuation of simulation. Parallelization: A parallel version of the code is available and open source. Piston: It is possible to use information from a piston type wavemaker. Flap: It is possible to use information from a flap type wavemaker. Time trace: It is possible to use time trace of wave elevation from a measurement station.

the wave elevation history at the measurement location closest to the wavemaker was used. Additionally, we carried out grid and time step refinement with the codes. The results presented in this paper were obtained from the convergence study. For the sake of brevity, details of the convergence study are not presented here, but some information about the grid and time step for each code in each test case will be given in the corresponding section.

In order to compare the performance of the codes, we will use both qualitative and quantitative information. For qualitative assessment, we will provide wave elevation histories at various measurement stations. For quantitative assessment, we will resort to analyzing wave elevation histories in order to calculate characteristics of the waves. The significant wave height H_{m_0}, variance quotient, correlation, and relative error in L_2 will be provided in tables. H_{m_0} is approximated as 4 times the square root of the variance. The correlation between the simulation and measurement is calculated by the 'cosine' correlation,

$$corr\left(\eta_e, \eta_s\right) = \frac{\eta_e \cdot \eta_s}{\|\eta_e\| \, \|\eta_s\|}. \tag{1}$$

This measures how well the experiment and the simulation align linearly, that is how well they point in the same direction. Therefore, this is especially useful to measure the phase shift errors in the simulation. The maximum value of 1 indicates that the simulation and the experiment are in phase, whereas the minimum value of -1 shows that the simulation is in counter phase with the experiment.

Additionally we will also use the relative error in L_2 between the measurement and the simulation,

$$\|\varepsilon\|_2 = \frac{\|\eta_e - \eta_s\|_2}{\|\eta_e\|_2}. \tag{2}$$

It is important to note that the relative error in L_2 may not be the ideal measure to compare the wave elevation from the simulation and experiment, since even small phase shifts can cause large error values. Nonetheless, it will give us an indication of the total error in the results.

We will also provide quantitative information particularly about the focused wave. In that respect we will pay attention to the crest height, trough depth, wave height, and time instance where the maximum amplitude occurs.

2.1 Wave groups propagating over a flat bottom

In this section we investigate the performance of the four codes in tests of propagating wave groups over a flat bottom. The tests consist of two focusing wave events, and a model scale of an irregular wave widely known as the Draupner wave or New Year's wave. The water depth is 1m and the length of the basin (from piston to the point where the beach intersects with the calm water surface) is 195.4m. The wave elevation was measured by six wave probes which were all located within the first 54m of the basin, see Tab. 2.

	W1	W2	W3	W4	W5	W6
Distance to wave generator (m)	10	20	40	49.5	50	54

Table 2: Location of the wave probes in the basin for the tests with a flat bottom.

2.1.1 Small-amplitude focusing wave (Experiment run number:202002)

Results for the test case 202002 were obtained using the following numerical settings. With SWASH, the grid resolution in the horizontal direction was $\Delta x = 0.01m$, and 20 layers were used in the vertical direction. CFL number was allowed to be between 0.2 and 0.5. With OceanWave3D, $\Delta x = 0.01m$, and 20 layers were used in the vertical direction with clustering towards the free surface. Half-width stencils were set to 3 and maximum CFL number was set to 0.5. With HOS-NWT, the number of point/modes were $N_x = 2048$, $N_z = 65$, and the HOS order was set to $M = 5$. Finally with HAWASSI, 2^{12} points were used in the simulations with a time step of $0.02s$.

At the measurement location W2, we observe that the wave signals from the four codes are overall similar as shown in Fig. 1a. However, it is possible to observe that HAWASSI, compared to the other three codes, slightly overestimates the wave heights, and results in slightly larger phase shifts especially for shorter waves.

At the measurement location W4 which is half a meter upstream of the focal point W5, we start to observe occurrence of a focussed wave as depicted in Fig. 1b. Focusing takes place at W5 as illustrated in Fig. 1c at $t = 109.34s$, and information about the focused waves at W4 and W5 is listed in Tab. 3. The results show that SWASH, OceanWave3D and HOS-NWT perform somewhat similarly. SWASH and HOS-NWT produce the smallest phase shift error. SWASH produces the smallest wave heights at both W4 and W5 underestimating both the crest height and trough depth of the focused waves. HAWASSI yields the largest phase shift and overestimates the trough depths at W4 and W5, however it estimates the crest heights more accurately than the other three codes at both locations. Considering both amplitude and phasing HOS-NWT performs better than SWASH and OceanWave3D.

		Experiment	HAWASSI	SWASH	OceanWave3D	HOS-NWT
W4	Crest (m)	0.046	0.044	0.042	0.041	0.043
	Trough (m)	-0.037	-0.04	-0.035	-0.038	-0.037
	Wave height (m)	0.083	0.084	0.077	0.079	0.08
	t_{peak} (s)	109.04	108.91	109.0	108.97	109.0
W5	Crest (m)	0.055	0.055	0.049	0.052	0.052
	Trough (m)	-0.025	-0.029	-0.024	-0.027	-0.025
	Wave height (m)	0.08	0.084	0.073	0.079	0.077
	t_{peak} (s)	109.34	109.22	109.33	109.3	109.33

Table 3: Maximum crest height, minimum trough depth, wave height, and time instance of the maximum amplitude from the measurement and simulations at W4 and W5 for the case 202002.

2.1.2 Large-amplitude focusing wave (Experiment run number:203001)

In the test case 203001, the same settings as the case 202002 were used for the four codes. Figure 2a displays wave signals from the experiment and the three codes at W2. Here, close observation of the wave signals reveals that SWASH performs slightly better than the other three codes yielding smaller phase shift, and estimating wave heights more accurately.

At the measurement locations W4 and W5 which are only half a meter apart from each other, we observe the focusing event as demonstrated in Figs. 2b and 2c. At both locations we detect

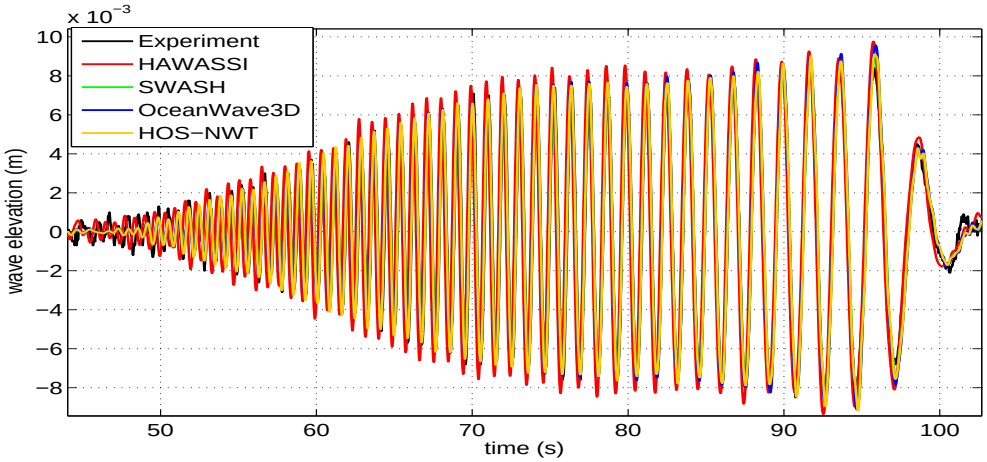

(a) W2

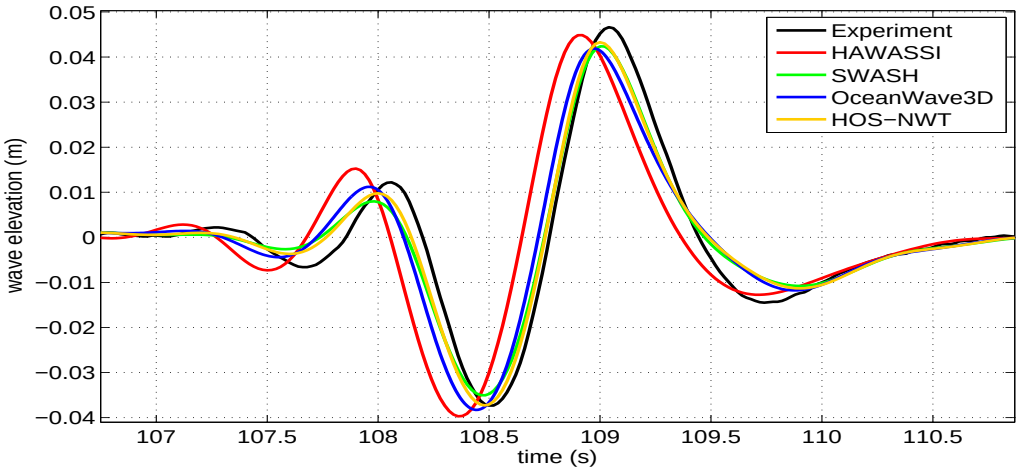

(b) W4

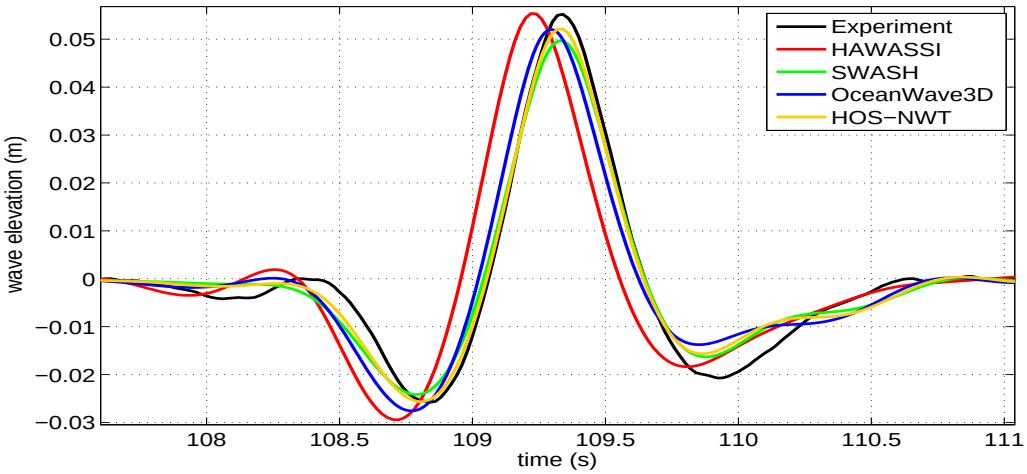

(c) W5

Figure 1: Comparison of the wave signals at the measurement location W2, W4 and W5 for the case 202002.

three peaks in the wave signals. Table 4 lists the information about the three peaks at W5, which occur at $t = 105.75s$, $t = 106.56s$, and $t = 107.86s$. For these three peaks HAWASSI results in the largest phase shift compared to the other codes. Analyzing the peaks occurring at $t = 106.24s$ and $t = 107.6s$ at W4 we observe that the wave crests are distorted in the wave signal from HOS-NWT. When we look at the wave profile of the highest peak occurring at $t = 107.86s$ at W5, we also notice some distortion in the wave crest from SWASH. For the highest peaks at both W4 and W5 the agreement between the OceanWave3D result and the experiment is good. Overall, OceanWave3D shows a better performance than the other three codes in this test case. In the simulations with HAWASSI and OceanWave3D the mechanisms to prevent wave breaking from happening were activated. With SWASH more than 10 layers in the vertical direction were used, and in the SWASH manual [13] it is mentioned that no additional measure needs to be taken in such a situation to account for wave breaking. With HOS-NWT no *ad hoc* measure was taken for wave breaking because HOS-NWT did not yet have a mechanism for this purpose. All these choices influenced the results inevitably, and the extent of this influence should not be underestimated. When the mechanisms for prevention of wave breaking are activated, the user is usually left to find a value for a *strength* parameter. Since there is not a clear guideline for the value of this parameter (typically there are only minimum and maximum limits), different values were chosen and their effects were observed. The results shown in this paper were those which were in the best agreement with the measurements.

		Experiment	HAWASSI	SWASH	OceanWave3D	HOS-NWT
P1	Crest (m)	0.029	0.054	0.012	0.038	0.040
	Trough (m)	-0.051	-0.062	-0.023	-0.059	-0.061
	Wave height (m)	0.08	0.116	0.035	0.097	0.101
	t_{peak} (s)	105.75	105.5	105.62	105.64	105.68
P2	Crest (m)	0.08	0.071	0.073	0.072	0.088
	Trough (m)	-0.079	-0.082	-0.102	-0.087	-0.072
	Wave height (m)	0.159	0.153	0.175	0.159	0.16
	t_{peak} (s)	106.56	106.32	106.6	106.42	106.44
P3	Crest (m)	0.106	0.102	0.093	0.099	0.113
	Trough (m)	-0.039	-0.043	-0.029	-0.038	-0.045
	Wave height (m)	0.145	0.145	0.122	0.137	0.158
	t_{peak} (s)	107.86	107.66	107.92	107.79	107.8

Table 4: Maximum crest height, minimum trough depth, wave height, and time instance of the three peaks at W5 for the case 203001.

2.1.3 The Draupner Wave (Experiment run number:204001)

The last test case over a flat bottom is the model scale of an irregular wave widely known as the Draupner Wave or New Year's wave. For this test case, the same settings as the case 202002 were used with SWASH and HOS-NWT, but we had several difficulties with OceanWave3D. The results from OceanWave3D were obtained on a grid with $\Delta x = 0.2m$, and 5 layers in the vertical direction. The time step was $0.02s$. Any attempt to refine the grid or change the time step was unsuccessful, as the solution diverged in all those attempts. This problem was reported

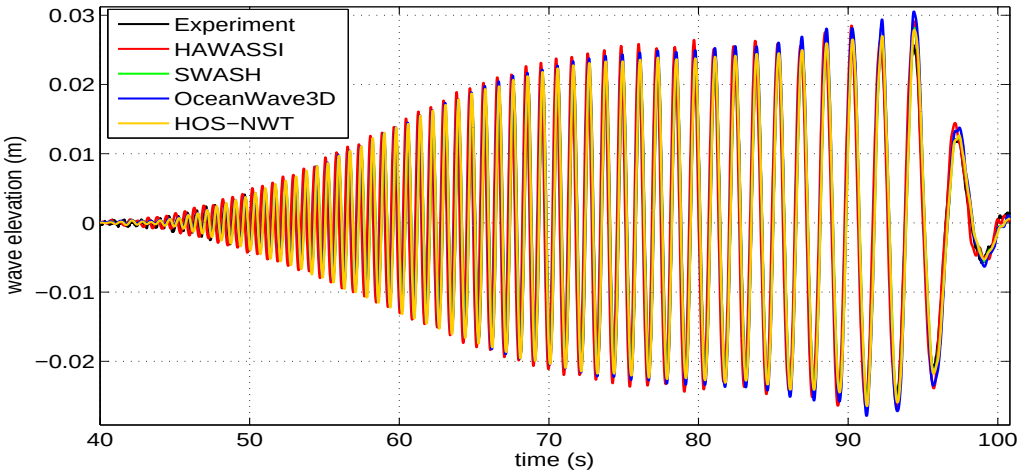

(a) W2

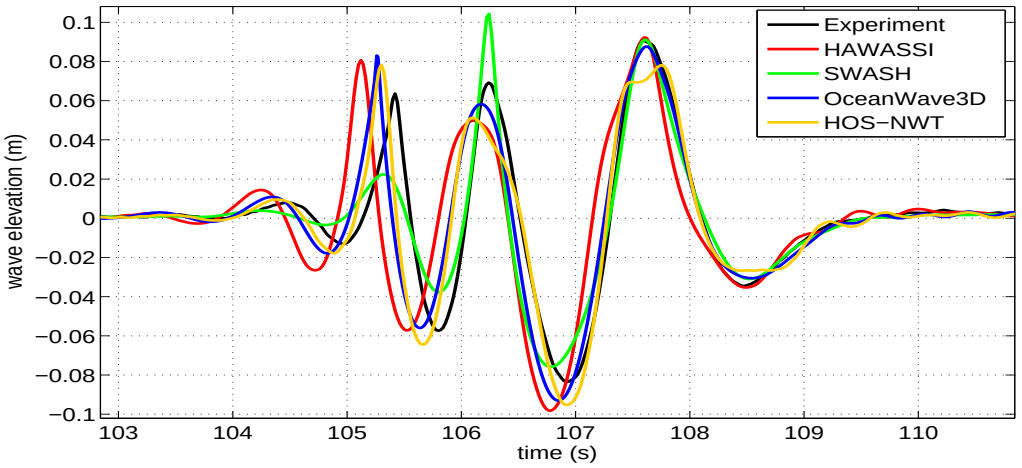

(b) W4

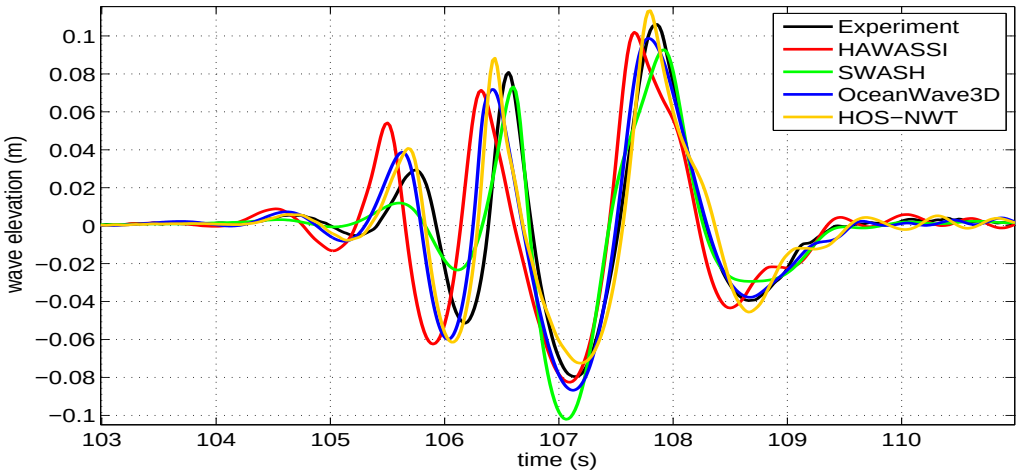

(c) W5

Figure 2: Comparison of the wave signals at the measurement location W2, W4 and W5 for the case 203001.

back to the developers of the OceanWave3D code. With HAWASSI, 2^{11} points were used in the simulations with a time step of $0.02s$.

At W2, W3, W4, W5 and W6, the wave signals from the three codes were analyzed, and the quantitative information about simulation accuracy is listed in Tab. 5. Similar to the test cases 202002 and 203001, a focussing event takes place in the case of 204001, and the wave probe W5 records the most extreme event occurring at $t = 164.6s$. The information about the focussed wave in particular is also provided in Tab. 6.

At the measurement station W2, we observe a good performance from all the codes resulting in at least 90% correlation with the experiment. Especially in the bottom plot of Fig. 3 where more energetic part of the wave group is illustrated, we observe a good agreement between the four simulations and the experiment. In the less energetic part of the wave group, however, we notice a clear difference between OceanWave3D and the other codes as shown in the middle plot of Fig. 3. This difference can be attributed to the low grid resolution in the OceanWave3D simulation, since these short and small waves are possibly not resolved on the grid. This also causes OceanWave3D to generate the highest relative error in L_2.

Among all the measurement stations, W5 records the most extreme event taking place at $t = 164.6s$. When we look at the values in Tab. 5, we see that OceanWave3D and HOS-NWT correspond with the experiment in a better fashion than SWASH and HAWASSI at W5. We notice this outcome also in the close-up view of the focusing event shown in the bottom plot of Fig. 4.

2.2 Wave groups propagating over a slope

In this section, we will present results from simulations with irregular waves propagating over a slope. These tests were not carried out with HOS-NWT since bathymetry effects had not been included in the model of HOS-NWT when this study was conducted. The geometrical setup, the details of the bathymetry, and the positions of the measurement stations are shown in Figure 5. The waves were generated with a piston-type wavemaker making only horizontal translations. 143.41m away from the wavemaker the slope with a steepness of 5% starts. The water depth in the deeper part is 0.6m, and the water depth in the shallower part is 0.3m. In the experiment, a beach is located at 173.41m away from the wavemaker. We will consider two test cases listed in Table 7. The duration of the experiment in both cases was nearly 1840s, but we carried out the simulations only for 500s which contains approximately 316 waves.

2.2.1 Test case:103001

Results for the test case 103001 were obtained using the following numerical settings. With SWASH, the grid resolution in the horizontal direction was $\Delta x = 0.025m$, and 20 layers were used in the vertical direction. CFL number was allowed to be between 0.2 and 0.5. With OceanWave3D, $\Delta x = 0.025m$, and 20 layers were used in the vertical direction with clustering towards the free surface. Half-width stencils were set to 2 and maximum CFL number was set to 0.5. Finally with HAWASSI, 2^{11} points were used in the simulations with a time step of $0.08s$.

At the measurement stations the wave signals were analyzed, and the quantitative information about simulation accuracy is listed in Table 8. We observe that HAWASSI underestimates wave heights at all measurement stations, while SWASH and OceanWave3D overestimate them. This can be seen in both H_{m_0} and variance quotient values from the three simulations. For this test case OceanWave3D generally shows better performance than the other codes producing

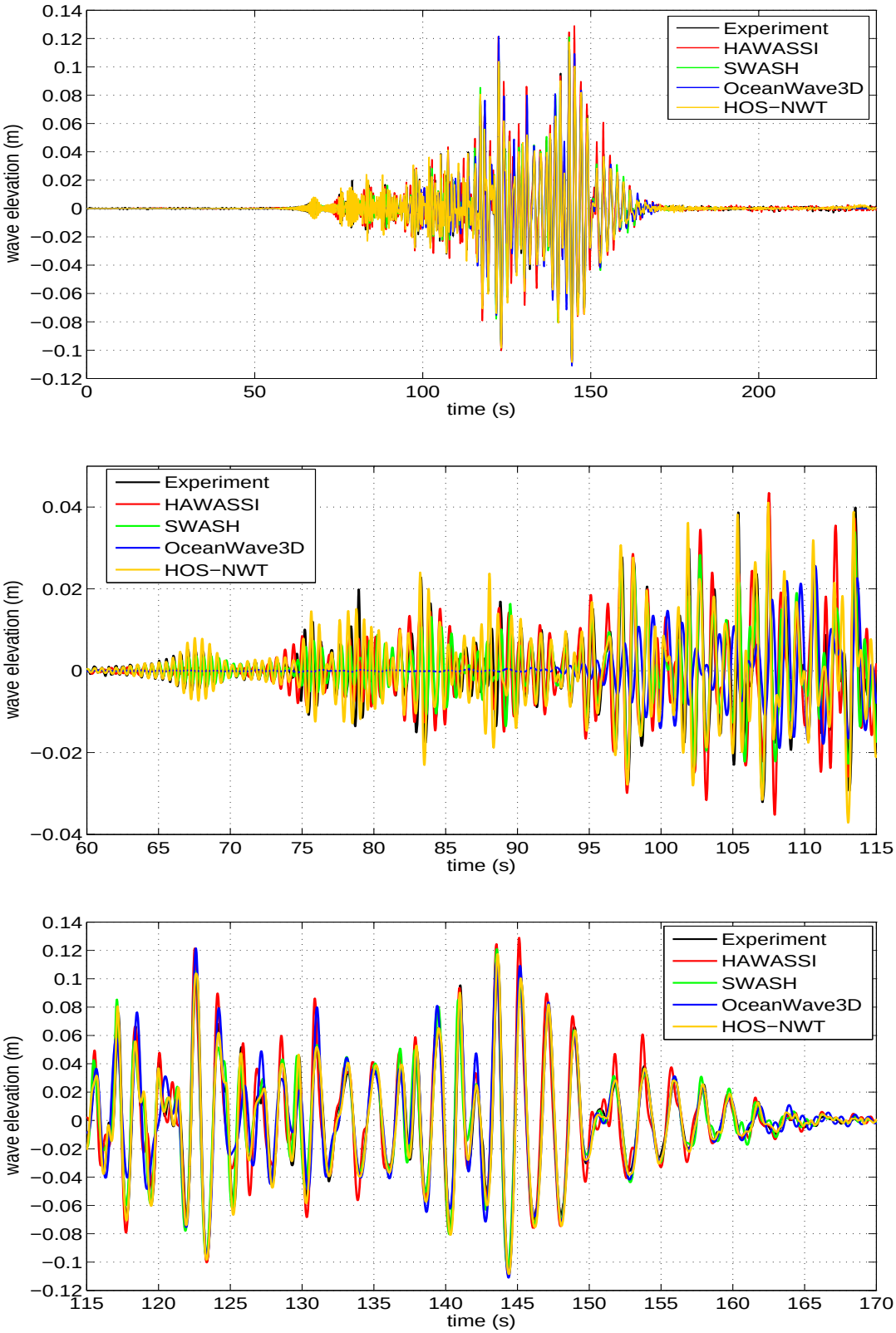

Figure 3: Comparison of the wave signals at the measurement location W2 for the case 204001. Top plot shows the complete time history, and the other two plots show close-up views of the two parts of the top plot.

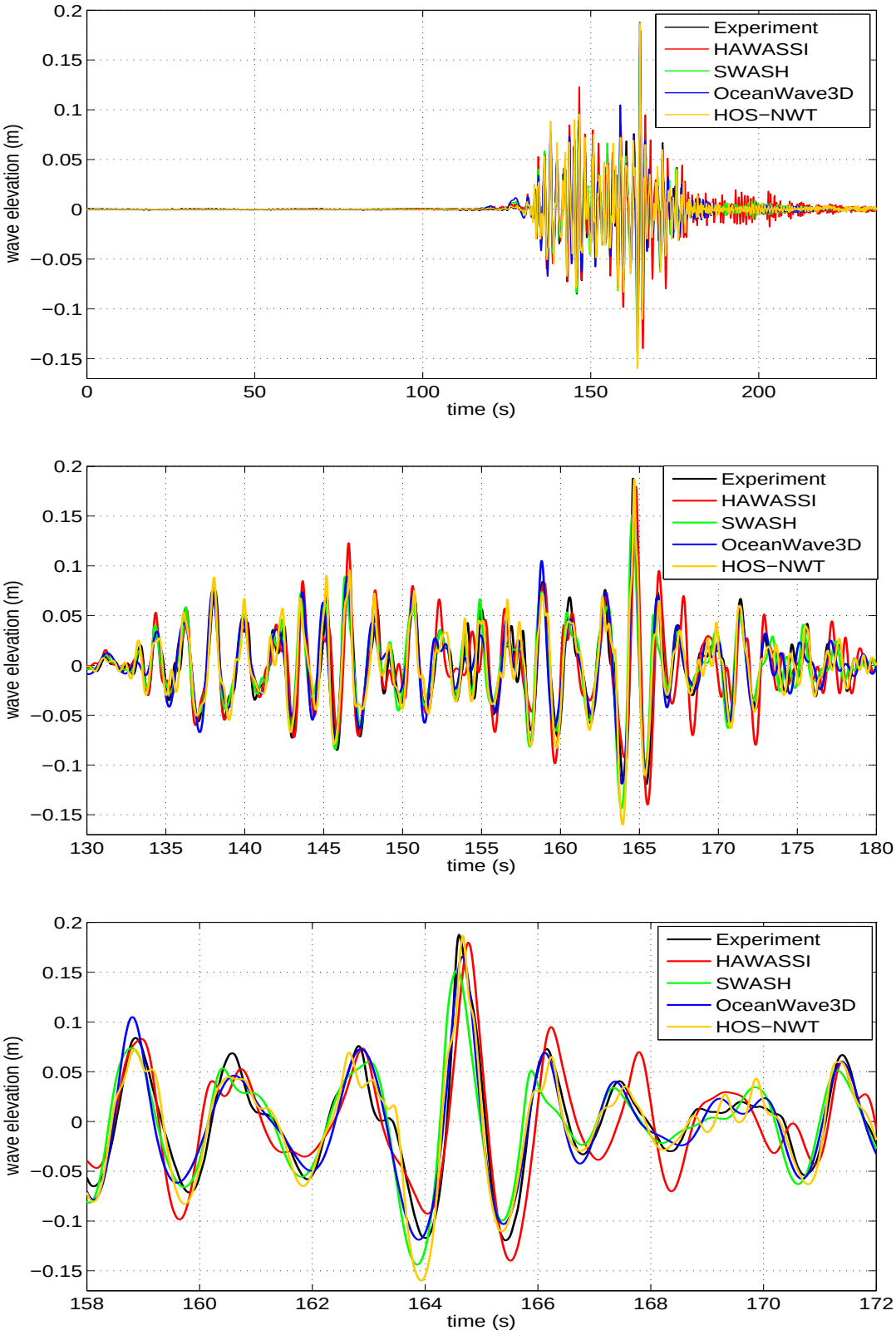

Figure 4: Comparison of the wave signals at the focal point W5 for the case 204001. Top plot shows the complete time history, middle plot shows the close-up view of the wave group, and the bottom plot shows the freak-like wave which occurs at $t = 164.6s$.

		HAWASSI	SWASH	OceanWave3D	HOS-NWT
W2	H_{m_0} (sim, exp) (m)	(0.075, 0.069)	(0.069, 0.069)	(0.070, 0.069)	(0.071, 0.069)
	Variance quotient	1.17	1.0	1.02	1.06
	Correlation	0.91	0.94	0.90	0.97
	L_2 norm	0.44	0.34	0.45	0.21
W3	H_{m_0} (sim, exp) (m)	(0.075, 0.072)	(0.067, 0.072)	(0.069, 0.072)	(0.070, 0.072)
	Variance quotient	1.07	0.87	0.92	0.95
	Correlation	0.87	0.87	0.88	0.93
	L_2 norm	0.52	0.50	0.48	0.36
W4	H_{m_0} (sim, exp) (m)	(0.075, 0.071)	(0.068, 0.071)	(0.069, 0.071)	(0.070, 0.071)
	Variance quotient	1.11	0.93	0.96	0.98
	Correlation	0.85	0.85	0.84	0.89
	L_2 norm	0.55	0.54	0.56	0.45
W5	H_{m_0} (sim, exp) (m)	(0.075, 0.07)	(0.068, 0.07)	(0.069, 0.07)	(0.071, 0.07)
	Variance quotient	1.15	0.94	0.97	1.03
	Correlation	0.84	0.87	0.89	0.91
	L_2 norm	0.58	0.50	0.45	0.42
W6	H_{m_0} (sim, exp) (m)	(0.074, 0.071)	(0.067, 0.071)	(0.069, 0.071)	(0.071, 0.071)
	Variance quotient	1.11	0.91	0.95	1.00
	Correlation	0.81	0.86	0.88	0.89
	L_2 norm	0.64	0.51	0.47	0.46

Table 5: Quantitative information concerning simulation accuracy for the case 204001.

	Experiment	HAWASSI	SWASH	OceanWave3D	HOS-NWT
Crest (m)	0.187	0.18	0.152	0.165	0.187
Trough (m)	-0.117	-0.092	-0.143	-0.119	-0.16
Wave height (m)	0.304	0.272	0.295	0.284	0.347
t_{peak} (s)	164.6	164.76	164.56	164.66	164.66

Table 6: Maximum crest height, minimum trough depth, wave height, and time instance of the maximum amplitude for the freak-like wave at W5 from the case 204001.

Run number	H_s (m)	T_p (s)
103001	$\cong 0.06$	1.697
104001	$\cong 0.06$	2.121

Table 7: Characteristics of the irregular waves propagating over a slope.

better correlation and smaller relative error in L_2. Measurement station W12 attracts our attention because this is where the three codes show their worst performance. Further investigation may be worthwhile to find an explanation for this observation.

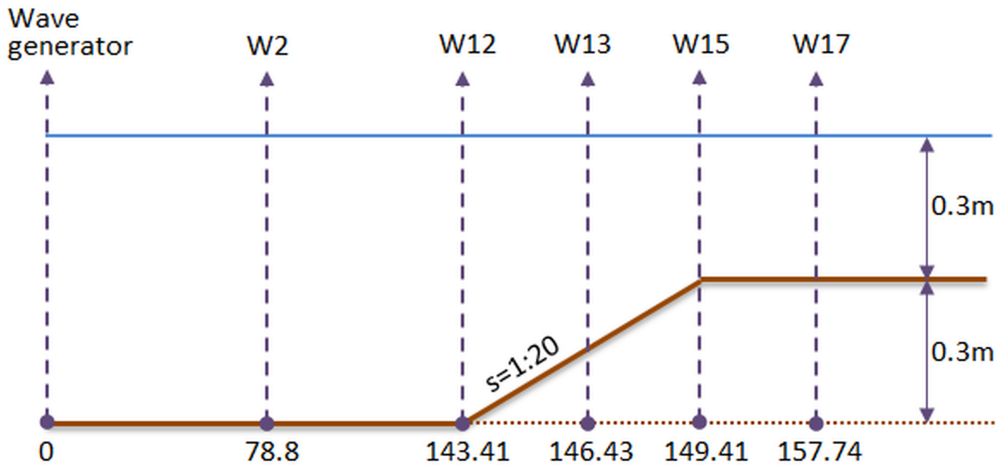

Figure 5: Setup of the experiment for the tests with irregular waves propagating over a slope. Piston-type wave generator is located at the left end of the basin. Wave elevations are measured at W2, W12, W13, W15 and W17. Slope has a steepness of 1:20. A beach is located at 173.41m away from the wavemaker (not shown in the figure). Distances are given in meters, and are not on scale.

		HAWASSI	SWASH	OceanWave3D
W2	H_{m_0} (sim, exp) (m)	(0.056, 0.06)	(0.063, 0.06)	(0.064, 0.06)
	Variance quotient	0.88	1.15	1.16
	Correlation	0.91	0.85	0.88
	L_2 norm	0.41	0.57	0.52
W12	H_{m_0} (sim, exp) (m)	(0.053, 0.054)	(0.059, 0.054)	(0.058, 0.054)
	Variance quotient	0.95	1.18	1.17
	Correlation	0.52	0.45	0.80
	L_2 norm	0.97	1.10	0.67
W13	H_{m_0} (sim, exp) (m)	(0.054, 0.056)	(0.06, 0.056)	(0.059, 0.056)
	Variance quotient	0.92	1.11	1.09
	Correlation	0.84	0.75	0.90
	L_2 norm	0.55	0.73	0.46
W15	H_{m_0} (sim, exp) (m)	(0.055, 0.06)	(0.062, 0.06)	(0.061, 0.06)
	Variance quotient	0.86	1.07	1.05
	Correlation	0.83	0.73	0.91
	L_2 norm	0.57	0.75	0.43
W17	H_{m_0} (sim, exp) (m)	(0.054, 0.058)	(0.054, 0.058)	(0.06, 0.058)
	Variance quotient	0.88	0.87	1.09
	Correlation	0.67	0.70	0.89
	L_2 norm	0.79	0.76	0.48

Table 8: Quantitative information concerning simulation accuracy for the case 103001.

2.2.2 Test case:104001

In the test case 104001, the same settings as the case 103001 were used for the three codes. Table 9 lists quantitative information about simulation accuracy based on the analysis of the wave signals at the measurement stations. HAWASSI, SWASH and OceanWave3D show a good agreement with the experiment at the measurement station W2. Here the correlation with the experiment is 95% with HAWASSI, 94% with SWASH, and 90% with OceanWave3D. As the wave propagates, we observe that both HAWASSI and SWASH fail to achieve these high correlation values at the other measurement stations. OceanWave3D, however, maintains high correlation values at all the five stations: 90% at W2, 88% at W12, 90% at W13, 91% at W15, and 89% at W17. Also, at W12, W13, W15 and W17 OceanWave3D yields much smaller errors in L_2 than the other two codes.

		HAWASSI	SWASH	OceanWave3D
W2	H_{m_0} (sim, exp) (m)	(0.06, 0.062)	(0.065, 0.062)	(0.064, 0.062)
	Variance quotient	0.92	1.10	1.06
	Correlation	0.95	0.94	0.90
	L_2 norm	0.32	0.37	0.45
W12	H_{m_0} (sim, exp) (m)	(0.058, 0.063)	(0.062, 0.063)	(0.061, 0.063)
	Variance quotient	0.84	0.98	0.96
	Correlation	0.64	0.60	0.88
	L_2 norm	0.82	0.89	0.49
W13	H_{m_0} (sim, exp) (m)	(0.06, 0.067)	(0.064, 0.067)	(0.063, 0.067)
	Variance quotient	0.80	0.91	0.90
	Correlation	0.85	0.78	0.90
	L_2 norm	0.53	0.64	0.43
W15	H_{m_0} (sim, exp) (m)	(0.063, 0.072)	(0.068, 0.072)	(0.067, 0.072)
	Variance quotient	0.76	0.88	0.87
	Correlation	0.85	0.76	0.91
	L_2 norm	0.53	0.67	0.42
W17	H_{m_0} (sim, exp) (m)	(0.062, 0.064)	(0.068, 0.064)	(0.067, 0.064)
	Variance quotient	0.96	1.13	1.11
	Correlation	0.71	0.66	0.89
	L_2 norm	0.76	0.85	0.48

Table 9: Quantitative information concerning simulation accuracy for the case 104001.

2.3 Summary and discussion

* For a comparative study in simulation of free surface water waves, four codes were selected: SWASH, OceanWave3D, HOS-NWT and HAWASSI. SWASH, OceanWave3D and HOS-NWT are open source and capable of running simulations in 3D, while HAWASSI requires a licence and can only run simulations in 2D. Nevertheless, a demo version of HAWASSI with fewer functionalities can be downloaded from its website.

* To assess their performance, a set of wave measurements is used; three wave groups propagating on a flat bottom and two irregular waves propagating on a slope. Since the design of HOS-NWT does not address varying bathymetry, this code is only used in the cases with flat bottom.

* The performance of HAWASSI in terms of computational cost is superior by a clear margin; in many cases the duration of simulation was close to the duration of real-time. This suggests that HAWASSI can be an ideal candidate to investigate statistics of extreme waves and wave groups. Computational cost of the other three codes was in the same order of magnitude. Therefore, a detailed analysis on this subject is not provided here. Even though grid and time step refinement studies were conducted, these were not presented here for the sake of brevity.

* In some cases, there were divergence issues with the OceanWave3D solution. At the time this paper was compiled, these issues were still not resolved. An important note is that when the solution diverges, the code does not stop the simulation, but rather continues until the end of the pre-specified simulation time. This is inconvenient, and it may inevitably waste computational resources.

* OceanWave3D allows using the velocity of only piston type wavemaker when the reproduction of basin waves is in question. This unfortunately limits the applicability of the code. Through personal communication OceanWave3D developers noted that there is currently no plan to include the use of flap type wavemaker information. This suggests that if this functionality is needed in a test case, either SWASH or HOS-NWT can be used.

* Various robustness issues were detected with SWASH. The code sometimes stops the simulation with a warning which does not give a clear indication of what went wrong. On the other hand, SWASH has some unique features, for example, it is the only code which can run a simulation on varying bathymetry using the information from a flap type wavemaker. SWASH also contains models for conservative transport of salinity, temperature and suspended sediment. The software has a well-written manual and an active user-community.

* HOS-NWT has some important limitations in functionality, for example, the code lacks a numerical workaround for wave breaking (through personal communication we were informed that the work on this subject is ongoing), and bathymetry effects are not incorporated into the model. Nevertheless the code showed a good performance in the test cases, and future improvements on its design will be monitored closely.

* Running simulations in parallel is an important functionality especially in 3D problems. One of the objectives in this work is to couple one of these codes with ReFRESCO which is mostly used in parallel. When ReFRESCO is run in parallel and the other code in serial, the efficiency of parallel computation may be compromised. At the moment only SWASH and OceanWave3D have parallel versions, and only SWASH has parallel open source version. Through personal communication OceanWave3D developers stated that the licence for the parallel version of OceanWave3D is not yet available.

* SWASH and OceanWave3D have the kinematics available in the entire domain at every time step. HOS-NWT and HAWASSI calculate the kinematics during a post-processing

step. This feature is an important requirement especially when coupling one of these codes with ReFRESCO is in question.

* Results indicate that none of the codes is clearly superior to the other ones especially in terms of accuracy. After an overall assessment of the codes based on their functionalities, accuracy, robustness and efficiency, OceanWave3D is selected for one-way coupling with ReFRESCO. However, the improvements on all the four models in the future will be monitored closely.

3 ONE-WAY COUPLING WITH REFRESCO

3.1 ReFRESCO Code

ReFRESCO (http://www.refresco.org) is a community based open-usage CFD code targeted for Maritime World problems. It solves multiphase (unsteady) incompressible viscous flows using the Navier-Stokes equations, complemented with turbulence models, cavitation models and volume-fraction transport equations for different phases [1] (in this particular case at hand both the air and water phases are modelled). The equations are discretized using a finite-volume approach with cell-centered collocated variables, in strong-conservation form, and a pressure-correction equation based on the SIMPLE algorithm is used to ensure mass conservation. The implementation is face-based, which permits grids with elements consisting of an arbitrary number of faces and if needed h-refinement (hanging nodes). Time integration is performed implicitly with first or second-order backward schemes. This means that there are no Courant number stability limitations, contrary to other codes used for tackling free-surface and wave problems [14]. However, small Courant numbers are important for a good balance between spatial and temporal discretizations, and also help the iterative convergence of the non-linear problem.

In a free-surface capturing method, such as the one here used, the discretization of the convective terms, both for momentum and volume-fraction transport equations, have an important effect in the robustness and in the accuracy of the solutions [15]. For the momentum a standard 2nd order unstructured-grids QUICK scheme is used. For the volume-fraction transport equation, it is known that in order to keep the free-surface interface sharp, compressive or anti-diffusive schemes have to be used [1]. In ReFRESCO one has several of these schemes, such as the well-known HRIC [16] and CICSAM [17]. However, these are Courant-number dependent and keep the compressive character only for Courant numbers lower than 1, which for an time-implicit code and for steady calculations is troublesome if not questionable. Therefore, in ReFRESCO, a compressive scheme ReFRICS is used for which the compressive character of the scheme is only based on the direction of the grid lines and the free-surface normal, and where there are no restrictions on the Courant number. For the rest of the discretization, the diffusion terms are treated using central schemes and the time derivatives using a three-time-level implicit scheme.

ReFRESCO (v2.2.0) is currently being developed, verified and its several applications validated at MARIN (in the Netherlands), in collaboration with IST (in Portugal), USP-TPN (University of Sao Paulo, Brasil), TUDelft (Technical University of Delft, the Netherlands), Soton (University of Southampton, UK), UTwente (University of Twente, the Netherlands) and Chalmers (Chalmers University, Sweden).

3.2 Coupling Procedure

For the sake of brevity we will not present the mathematical and numerical designs of OceanWave3D and ReFRESCO. For this purpose several references were previously mentioned. For one-way coupling of OceanWave3D with OpenFOAM®, see [18].

The information transfer from OceanWave3D to ReFRESCO takes place only at the inflow boundary of ReFRESCO, see Fig. 6. This transfer can be carried out in two ways:

1. One-way coupling of the two codes: Solutions in both codes advance in time simultaneously, and ReFRESCO calls OceanWave3D at every time step to receive the flow information. This information is then interpolated onto the inflow boundary of ReFRESCO.

2. Running simulation in each code separately and consecutively: First the simulation is performed using the potential flow solver, and the flow information in the relevant part of the domain is stored to a file. Secondly this file is read by ReFRESCO to assign values to the flow variables at the inflow boundary. Any one of the three codes (SWASH, OceanWave3D and HOS-NWT) can very well be used in the first step as long as all the necessary flow information is outputted and stored to a file. This method allows ReFRESCO to have a very flexible environment in order to generate waves. Furthermore, since the complete solution history is at the disposal of the user before starting the simulation in ReFRESCO, a certain part of that history can be cropped and sent into ReFRESCO instead of the complete history.

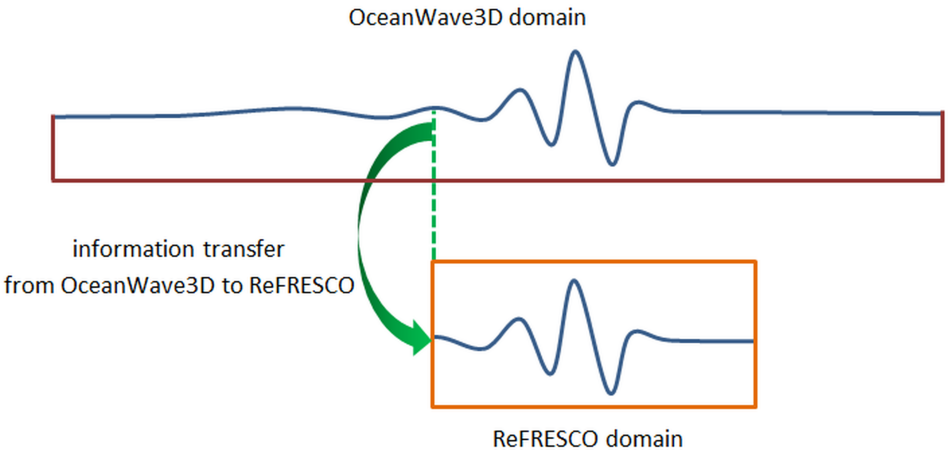

Figure 6: An example layout of the OceanWave3D and ReFRESCO domains, and the one-way coupling.

Both methods should produce the same result since the information that is transferred into ReFRESCO is essentially the same, only the way it is transferred changes. Therefore, in the remainder of this paper we will show results from only the first method.

In this method solutions in both codes advance in time simultaneously, and ReFRESCO calls OceanWave3D at every time step to receive the flow information. This information is then interpolated onto the inflow boundary of ReFRESCO. Both codes use the same time step, therefore no interpolation in time is necessary between the two solutions. At the beginning of each time step, the velocity and free surface elevation values are received from OceanWave3D, and imposed at the inflow boundary of the ReFRESCO domain. Since both codes use different

computational grids, the information from OceanWave3D has to be interpolated onto the grid of ReFRESCO. This is the only interpolation procedure used in the entire one-way coupling of both codes. The interpolation is done in the computational domain of OceanWave3D. The target value of a flow quantity $\psi_{target}\left(\boldsymbol{x}+\delta \boldsymbol{e}_i\right)$ at the location $\boldsymbol{x}+\delta \boldsymbol{e}_i$ whose nearest neighbour point located at $\boldsymbol{x}$ is calculated using the following finite Taylor series

$$\psi_{target}\left(\boldsymbol{x}+\delta \boldsymbol{e}_i\right)=\sum_{n=0}^{2a} \frac{\delta^n}{n!} \frac{\partial^n \psi}{\partial x_i^n}(\boldsymbol{x}) \tag{3}$$

where a is user-defined. The gradients $\partial^n \psi / \partial x_i^n$ were computed previously during the discretization of the governing equations. The number of terms in the Taylor series, $2a+1$, is consistent with the size of the finite difference stencil of the solver. Therefore both the Taylor series and the computed wave solution have a consistent numerical discretization error.

3.3 Results from the ReFRESCO-OceanWave3D coupling

In order to refer to OceanWave3D/ReFRESCO coupling, simply ReFRESCO will be used in the remainder of this document. A close-up view of a typical grid used in the simulations with ReFRESCO is shown in Fig. 7. The grid is finely spaced near the undisturbed interface between water and air, but becomes coarser towards the bottom and top boundaries of the domain. Along the horizontal direction no grid stretching was applied. The size of the grid cells near the undisturbed interface is given below in each test case.

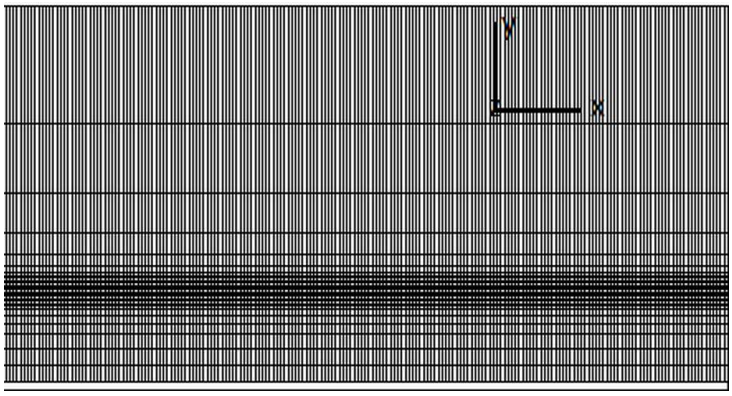

Figure 7: Close-up view of a typical grid used for the wave simulations.

In all the test cases, a three-level time discretization scheme is used. The time step was fixed throughout the simulations for all equations. Convergence tolerance is set to 10^{-4} for the infinity norm of the residuals of all the flow variables. In order to achieve such a residual decrease, the maximum value for the number of outer loops was set to 150.

The momentum and volume fraction equations are solved using GMRES with BJACOBI preconditioner, while the pressure correction equation is solved using CG with BJACOBI preconditioner. No turbulence model is used.

Dynamic viscosity of water is set to $1.002 \times 10^{-3} kg \cdot m^{-1} \cdot s^{-1}$, and air to $1.824 \times 10^{-5} kg \cdot m^{-1} \cdot s^{-1}$. For the density values of water and air, $998 kg \cdot m^{-3}$ and $1.118 kg \cdot m^{-3}$ are used, respectively.

The same boundary conditions are used in all the simulations with ReFRESCO, which are shown in Fig. 8. The outflow boundary, where the Sommerfeld boundary condition [19] is

applied, is positioned in such a way that reflected waves do not disturb the solution in the part of the domain where wave probes are located.

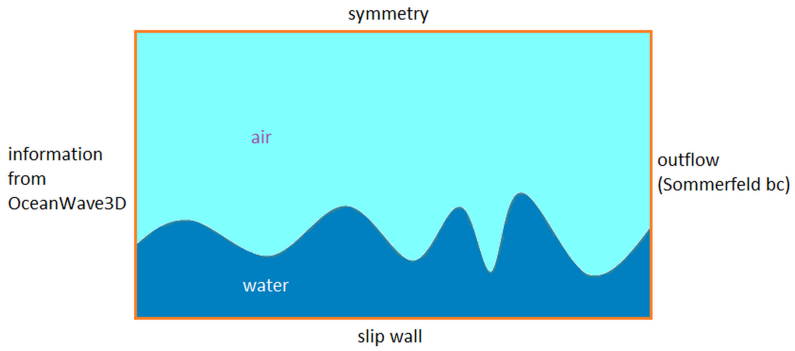

Figure 8: Boundary conditions for the simulations with ReFRESCO.

3.3.1 Small-amplitude focusing wave (Experiment run number:202002)

The wave probe W3 is the inflow boundary of ReFRESCO, where the quantities from OceanWave3D are imposed, see Tab. 2 for the locations of the wave probes. Three grid resolutions are considered with ReFRESCO: $(\Delta x = 0.04m,\ \Delta z = 0.016m)$, $(\Delta x = 0.02m,\ \Delta z = 0.008m)$, and $(\Delta x = 0.01m,\ \Delta z = 0.004m)$. Time step size is equal to 0.005s, and the simulation is carried out for 120s.

Figure 9 shows the wave signals at the measurement stations W4 and W5. We observe that the result on the coarse grid shows relatively larger deviations in terms of both wave height and phase shift compared to the medium and fine grids. The results on the medium and fine grids are, however, considerably similar and in good agreement with the measurement.

The residual history with time is plotted in Fig. 10 for the three grid resolutions. Note that only the last residual value for each time step is plotted for all the flow variables. The residuals for all the flow variables generally decrease around 5 orders of magnitude on all the three grids. The only exception to this is observed on the fine grid between $t = 107s$ and $t = 111s$, where 3.5 orders of magnitude decrease is achieved for some time levels, see Fig. 10c. When we look at the wave elevation histories from the wave probes W4 and W5, we notice that this time window coincides with the focusing event. During the focusing event the flow exhibits the highest velocities, which results in a considerable increase in the CFL number, see Fig. 11. This can be the cause for the relatively higher residuals on the fine grid. Small CFL numbers observed for the large part of the simulation result in small discretization errors and help the iterative convergence of the non-linear problem.

3.3.2 Large-amplitude focusing wave (Experiment run number:203001)

Similar to the previous test case, the wave probe W3 is the inflow boundary of ReFRESCO, where the quantities from OceanWave3D are imposed, see Tab. 2 for the locations of the wave probes. Three grid resolutions are considered with ReFRESCO: $(\Delta x = 0.04m,\ \Delta z = 0.024m)$, $(\Delta x = 0.02m,\ \Delta z = 0.012m)$, and $(\Delta x = 0.01m,\ \Delta z = 0.006m)$. Time step size is equal to 0.005s, and the simulation is carried out for 120s.

Similar to the test case 202002, the coarse grid seems inadequate as deviations from the experiment are relatively larger compared to the other two grids, see Fig. 12. It can also

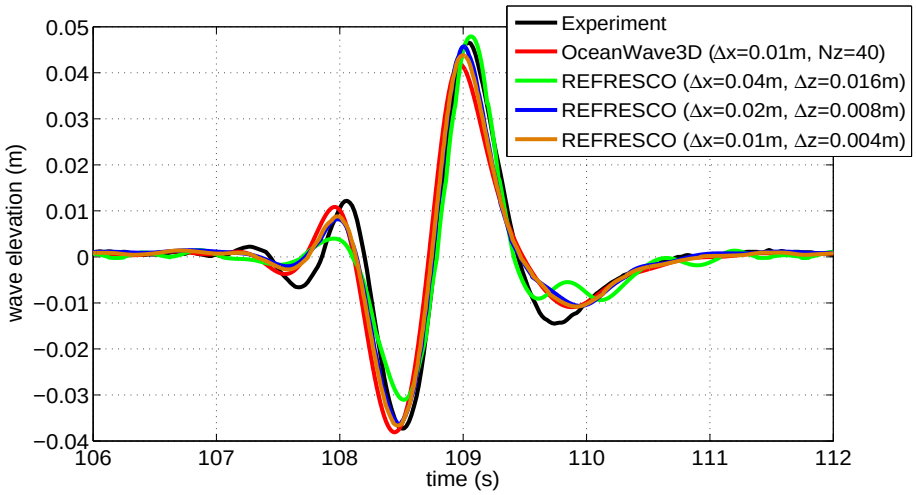

(a) W4

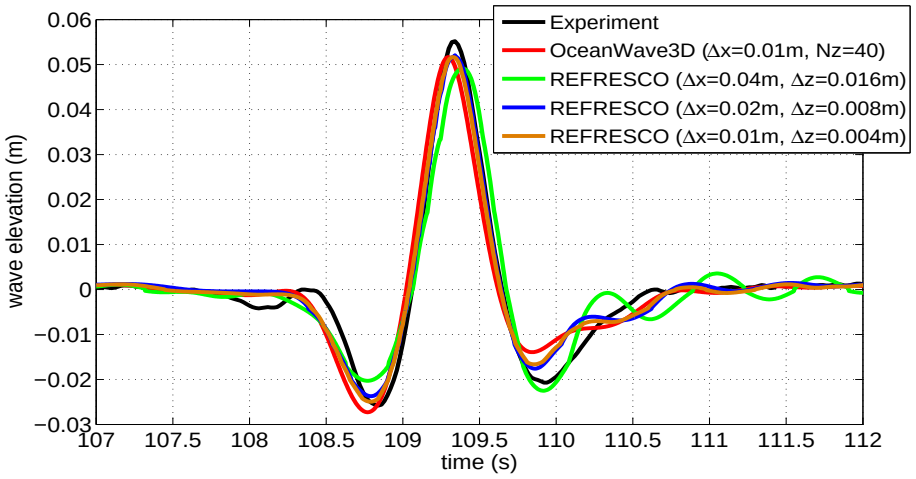

(b) W5

Figure 9: Comparison of the wave signals at the measurement locations W4 and W5 for the case 202002.

be observed that no further grid refinement is necessary as the results from the medium and fine grids are considerably close. The agreement between the experiment and ReFRESCO simulations on the medium and fine grids is acceptable.

The residual history with time is plotted in Fig. 13 for the coarse grid with the resolution of $(\Delta x = 0.04m,\ \Delta z = 0.024m)$. On this grid we observe that nearly 5 orders of magnitude decrease in error is achieved for almost the entire simulation. However, for some time levels, we observe a temporary increase in residuals. Even though not shown here, this increase becomes more pronounced on the medium and fine grids, and the residuals decrease at approximately 3 order of magnitude on these two grids. These relatively high errors take place around the focusing event where high velocities are observed in the simulation. This results in a sharp increase in the CFL number which almost reaches the value of 6 on the fine grid, see Fig. 14. Even though the order of magnitude of the residuals can be acceptable for wave simulations, an investigation into possible modifications in the settings of the solvers for a better convergence behavior can be worthwhile.

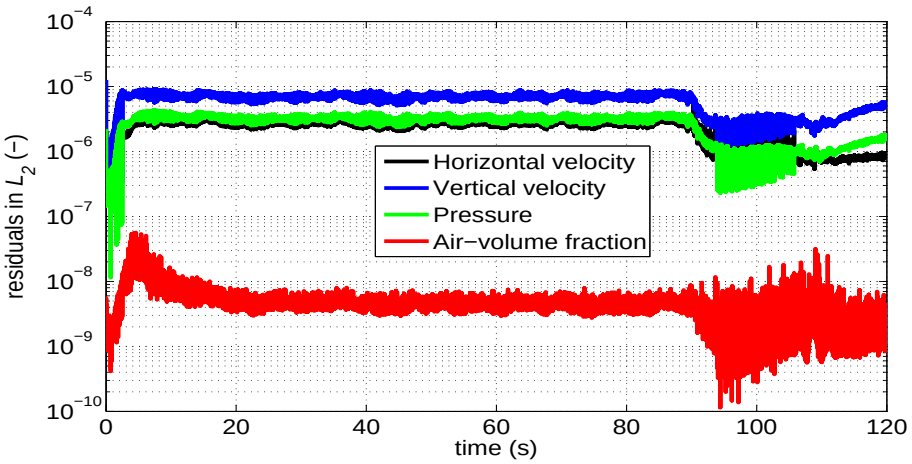

(a) Coarse grid ($\Delta x = 0.04m, \Delta z = 0.016m$)

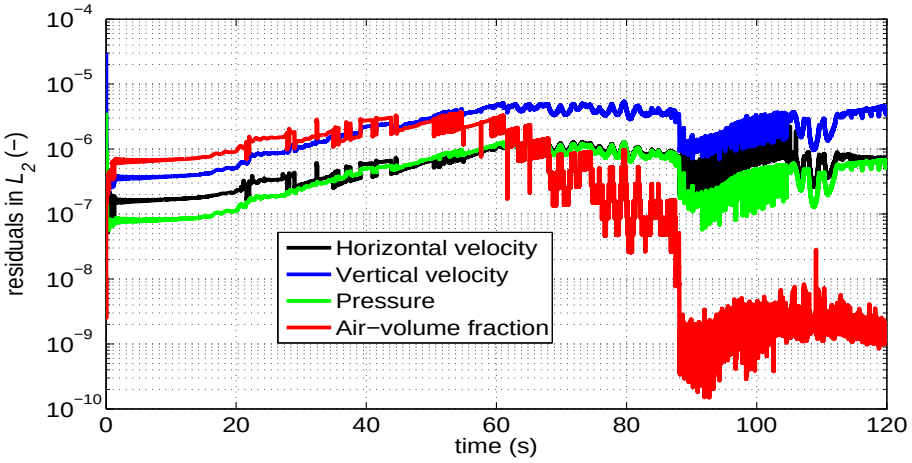

(b) Medium grid ($\Delta x = 0.02m, \Delta z = 0.008m$)

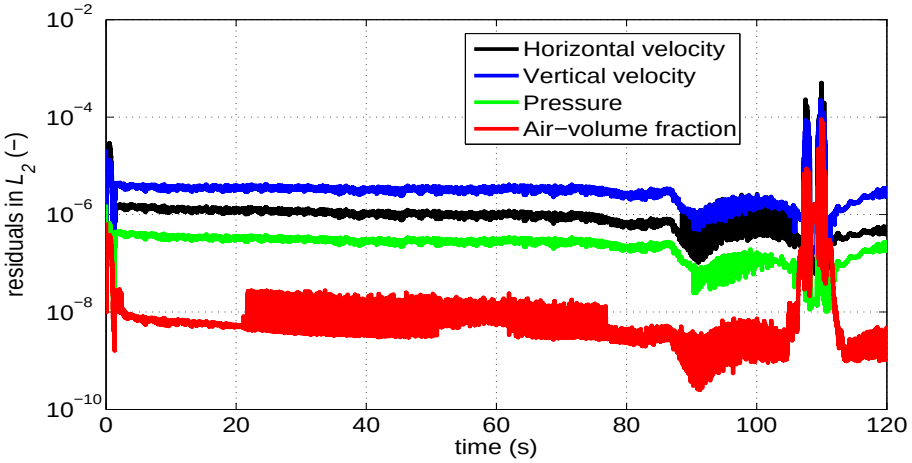

(c) Fine grid ($\Delta x = 0.01m, \Delta z = 0.004m$)

Figure 10: Residuals in L_2 on the three grid resolutions for the case 202002.

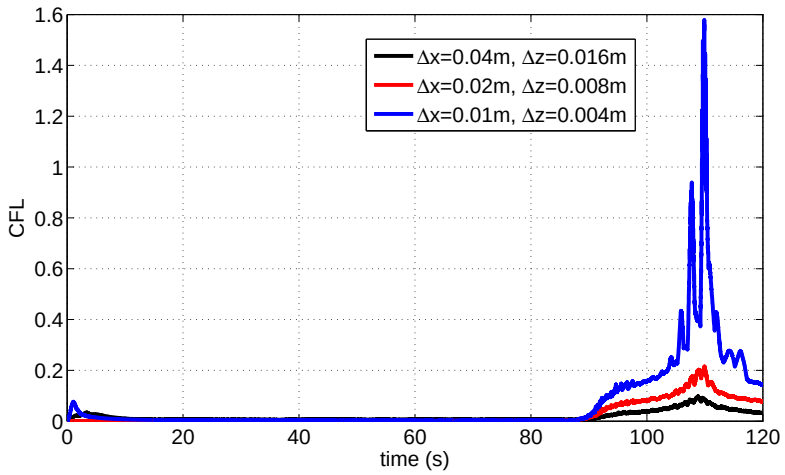

Figure 11: History of CFL number on the three grid resolutions for the case 202002.

4 CONCLUSIONS

* In this study several objectives were set and realized. The first objective was to conduct an inventory study on the existing potential flow codes which can be used for simulating nonlinear waves. Then an overall assessment of these codes had to be made in order to explore their features and investigate their performances. The final objective was to use these codes in order to generate waves in ReFRESCO.

* After a survey on the existing models, four codes were selected: SWASH, OceanWave3D, HOS-NWT and HAWASSI. The functionalities and performances of these codes were analyzed. After careful consideration, OceanWave3D was selected for one-way coupling with ReFRESCO.

* Various simulations were carried out with the ReFRESCO\OceanWave3D coupling. Grid refinement study was conducted and convergence behavior of ReFRESCO was monitored. Results indicated that the ReFRESCO\OceanWave3D coupling is a valuable tool to investigate wave motion in an accurate and efficient manner. In all the simulations, comparison with the measurements demonstrated good agreement, and the convergence behavior of ReFRESCO was acceptable.

* Future work will include testing the ReFRESCO\OceanWave3D coupling in various 3D problems particularly focusing on hydrodynamic wave loading on structures and wave-structure interaction.

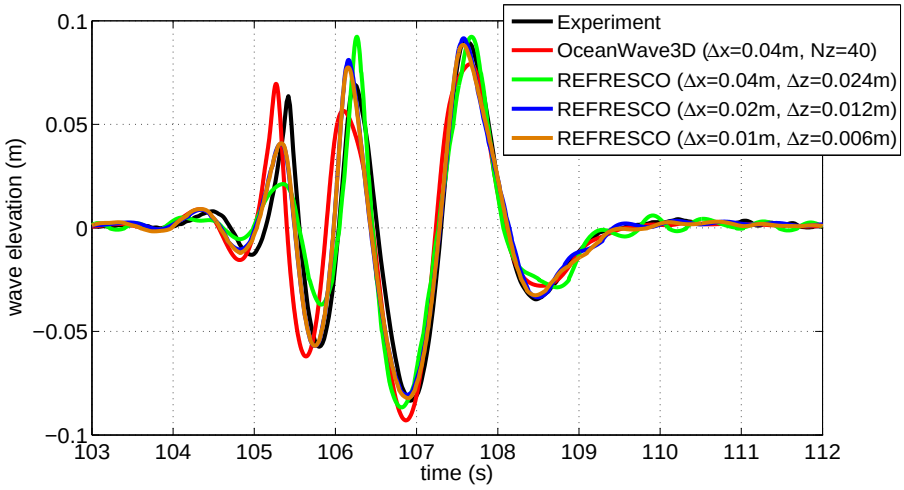

(a) W4

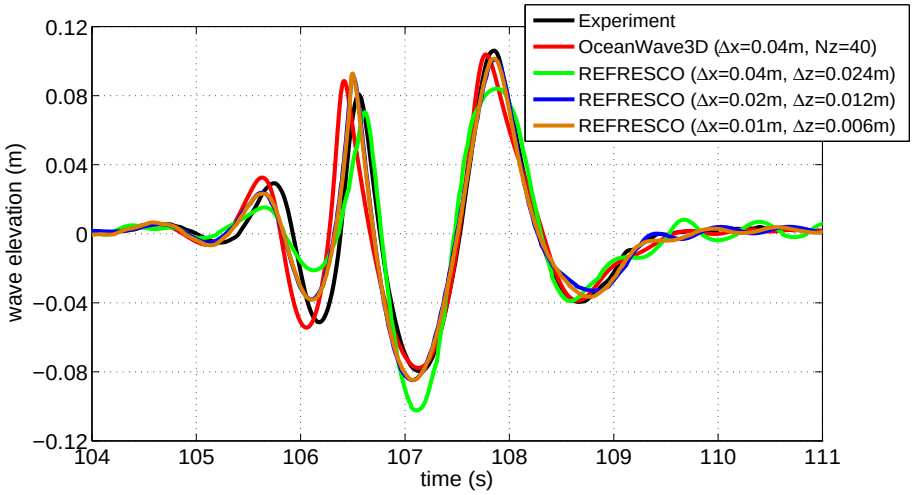

(b) W5

Figure 12: Comparison of the wave signals at the measurement locations W4 and W5 for the case 203001.

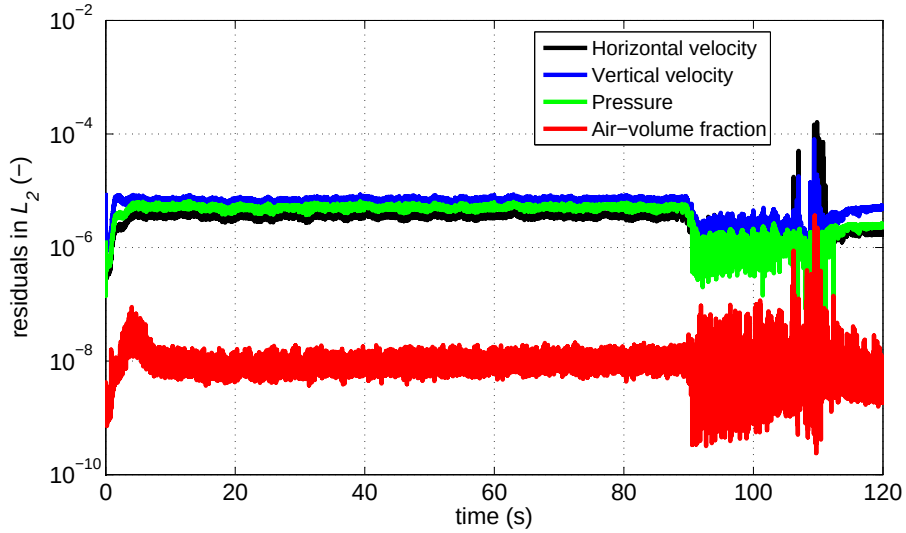

Figure 13: Residuals in L_2 on the coarse grid with the resolution of $(\Delta x = 0.04m, \Delta z = 0.024m)$ for the case 203001.

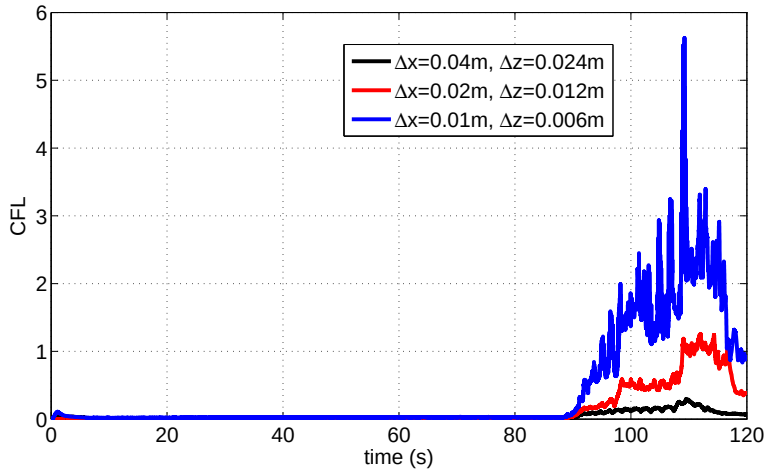

Figure 14: History of CFL number on three grid resolutions for the case 203001.

REFERENCES

[1] Vaz, G., Jaouen, F., and Hoekstra, M., 2009. "Free-surface viscous flow computations. Validation of URANS code FRESCO". In Proc. ASME 2009 28th International Conference on Ocean, Offshore and Arctic Engineering OMAE2009, Vol. 5, paper OMAE2009-79398.

[2] Liam, L. S., Adytia, D., and van Groesen, E., 2014. "Embedded wave generation for dispersive surface wave models". *Ocean Engineering,* ***80***, pp. 73 – 83.

[3] Kurnia, R., and van Groesen, E., 2014. "High order Hamiltonian water wave models with wave-breaking mechanism". *Coastal Engineering,* ***93***, pp. 55 – 70.

[4] van Groesen, E., and Andonowati, 2011. "Fully dispersive dynamic models for surface water waves above varying bottom, Part 1: Model equations". *Wave Motion,* ***48***(7), pp. 658 – 667.

[5] van Groesen, E., and van der Kroon, I., 2012. "Fully dispersive dynamic models for surface water waves above varying bottom, Part 2: Hybrid spatial-spectral implementations". *Wave Motion,* ***49***(1), pp. 198 – 211.

[6] Stelling, G., and Zijlema, M., 2003. "An accurate and efficient finite-difference algorithm for non-hydrostatic free-surface flow with application to wave propagation". *International Journal for Numerical Methods in Fluids,* ***43***(1), pp. 1–23.

[7] Stelling, G. S., and Duinmeijer, S. P. A., 2003. "A staggered conservative scheme for every Froude number in rapidly varied shallow water flows". *International Journal for Numerical Methods in Fluids,* ***43***(12), pp. 1329–1354.

[8] Zijlema, M., and Stelling, G. S., 2005. "Further experiences with computing non-hydrostatic free-surface flows involving water waves". *International Journal for Numerical Methods in Fluids,* ***48***(2), pp. 169–197.

[9] Zijlema, M., and Stelling, G., 2008. "Efficient computation of surf zone waves using the nonlinear shallow water equations with non-hydrostatic pressure". *Coastal Engineering,* ***55***(10), pp. 780 – 790.

[10] Engsig-Karup, A., Bingham, H., and Lindberg, O., 2009. "An efficient flexible-order model for 3D nonlinear water waves". *Journal of Computational Physics,* ***228***(6), pp. 2100 – 2118.

[11] Ducrozet, G., Bonnefoy, F., Touzé, D. L., and Ferrant, P., 2012. "A modified High-Order Spectral method for wavemaker modeling in a numerical wave tank". *European Journal of Mechanics - B/Fluids,* ***34***, pp. 19 – 34.

[12] Bonnefoy, F., Ducrozet, G., Touzé, D. L., and Ferrant, P., 2009. "Time-domain simulation of nonlinear water waves using spectral methods". In *Advances in numerical simulation of nonlinear water waves*, Q. Ma, ed. World Scientific, ch. 11, pp. 129–164.

[13] SWASHteam, 2010. *SWASH User Manual*. Delft University of Technology.

[14] Düz, B., 2015. "Wave generation, propagation and absorption in CFD simulations of free surface flows". PhD thesis, Delft University of Technology, The Netherlands.

[15] Kerkvliet, M., Vaz, G., Carette, N., and Gunsing, M., 2014. "Analysis of U-type anti-roll tank using URANS. sensitivity and validation". In Proc. ASME 2014 33rd International Conference on Ocean, Offshore and Arctic Engineering OMAE2014, Vol. 2, paper OMAE2014-23483.

[16] Muzaferija, S., Peric, M., Sames, P., , and Schelin, T., 1998. "A two-fluid Navier-Stokes solver to simulate water entry". In Proc. 22nd Symposium on Naval Hydrodynamics.

[17] Ubbink, O., and Issa, R., 1999. "Method for capturing sharp fluid interfaces on arbitrary meshes". *Journal of Computational Physics,* ***153***, pp. 26–50.

[18] Paulsen, B. T., Bredmose, H., and Bingham, H. B., 2014. "An efficient domain decomposition strategy for wave loads on surface piercing circular cylinders". *Coastal Engineering,* ***86***, pp. 57 – 76.

[19] Sommerfeld, A., 1949. *Partial differential equations in physics*. Academic Press.